Epilepsy & Behavior 97 (2019) 219–228

Contents lists available at ScienceDirect

Epilepsy & Behavior

journal homepage: www.elsevier.com/locate/yebeh

Genetic absence epilepsy: Effective connectivity from piriform cortex to mediodorsal thalamus

James C. Young [a,b,*], Antonio G. Paolini [a,b,d,e], Mangor Pedersen [a], Graeme D. Jackson [a,b,c]

[a] The Florey Institute of Neuroscience and Mental Health, Melbourne, Australia
[b] Florey Department of Neuroscience and Mental Health, The University of Melbourne, Melbourne, Australia
[c] Department of Neurology, Austin Health, Melbourne, Australia
[d] ISN Psychology — Institute for Social Neuroscience, Melbourne, Australia
[e] School of Psychology and Public Health, La Trobe University, Melbourne, Australia

ARTICLE INFO

Article history:
Received 23 January 2019
Revised 24 May 2019
Accepted 28 May 2019
Available online 26 June 2019

Keywords:
Absence epilepsy
Effective connectivity
Transfer entropy
Mediodorsal thalamus
Piriform cortex

ABSTRACT

Objective: The objective of the study was to quantify effective connectivity from the piriform cortex to mediodorsal thalamus, in Genetic Absence Epilepsy Rats from Strasbourg (GAERS).
Methods: Local field potentials (LFPs) were recorded using microelectrode arrays implanted in the mediodorsal thalamus and piriform cortex, in three urethane anesthetized GAERS and three control rats. Screw electrodes were placed in the primary motor cortex to identify epileptiform discharges. We used *transfer entropy* to measure effective connectivity from piriform cortex to mediodorsal thalamus prior to and during generalized epileptiform discharges.
Results: We observed increased theta band effective connectivity from piriform cortex to mediodorsal thalamus, prior to and during epileptiform discharges in GAERS compared with controls. Increased effective connectivity was also observed in beta and gamma bands from the piriform cortex to mediodorsal thalamus, but only during epileptiform discharges.
Conclusions: This preliminary study suggests that increased effective theta connectivity from the piriform cortex to the mediodorsal thalamus may be a feature of the 'epileptic network' associated with genetic absence epilepsy. Our findings indicate an underlying predisposition of this direct pathway to propagate epileptiform discharges in genetic absence epilepsy.

1. Introduction

Genetic absence epilepsy is a common form of childhood epilepsy [1] associated with absence seizures that are generalized epileptic events that cause a brief loss of consciousness [2]. Absence seizures are characterized by generalized spike–wave discharges (SWDs) (5–9 Hz in animal models, 3–5 Hz in humans) detected with electroencephalography (EEG) recordings. Animal studies have shown that the layer 5/6 of perioral somatosensory cortex likely generates absence seizure activity [3–5] that can be readily propagated via cortico-thalamic-cortico pathways [6,7]. While there has been a strong focus on corticothalamic mechanisms of absence epilepsy, there has been less focus on the role of limbic structures in absence epilepsy. Recent studies have shown abnormalities in mesial temporal regions such as the hippocampus, amygdala, and piriform cortex in both animal models of absence epilepsy [8–12] and human patients with absence epilepsy [13,14]. The piriform cortex is highly susceptible to hyperexcitable neuronal activity [15]. It also exhibits increased blood flow in Genetic Absence Epilepsy Rats from Strasbourg (GAERS), a well-established model of absence epilepsy [16–18], compared with nonepileptic controls (NECs) [8]. Increased blood flow was observed in the somatosensory cortex and ventrobasal thalamus as well as amygdala, entorhinal cortex, and hippocampus (CA2). This suggests that there may be a relationship between thalamocortical and limbic structures in absence epilepsy [12]. There is also clinical evidence of bilateral activation of the piriform cortex occurring synchronously with generalized SWDs in patients with absence epilepsy [13], however, it is unknown if there is any subtle changes in activity prior to the onset of seizures. Furthermore, the piriform cortex displays several anatomical pathways that link it to key regions associated with the absence epilepsy network [19] including unidirectional excitatory projections to the mediodorsal thalamus [20–24]. The mediodorsal thalamus is a higher-order thalamic nucleus

Abbreviations: EEG, electroencephalography; GAERS, Genetic Absence Epilepsy Rats from Strasbourg; LFPs, local field potentials; NECs, nonepileptic controls; SWD, spike–wave discharge.

* Corresponding author at: The Florey Institute of Neuroscience and Mental Health, Melbourne Brain Centre, 245 Burgundy Street, Heidelberg, Victoria 3084, Australia.
E-mail address: james.young@unimelb.edu.au (J.C. Young).

https://doi.org/10.1016/j.yebeh.2019.05.042
1525-5050/

Electrode Implantation Sites

A) Mediodorsal Thalamus Electrode Placement – Coronal View

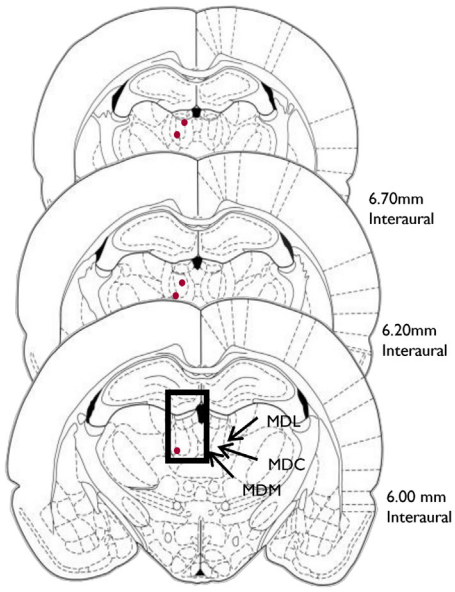

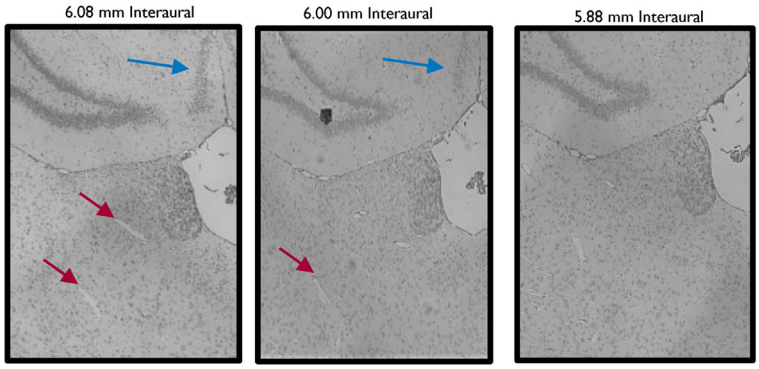

B) Piriform Cortex Electrode Placement – Coronal View

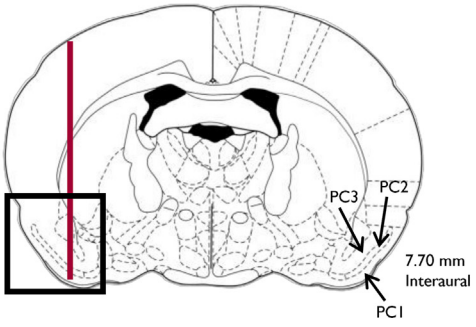

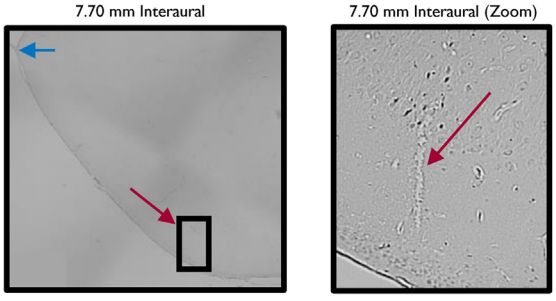

C) Electrode Placement – Sagittal View Reconstruction

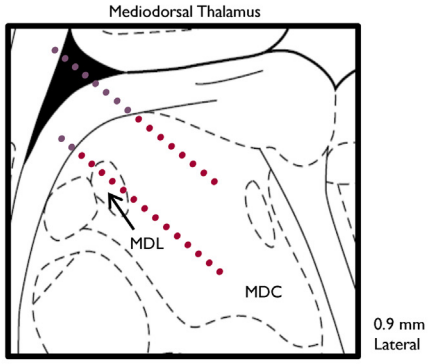

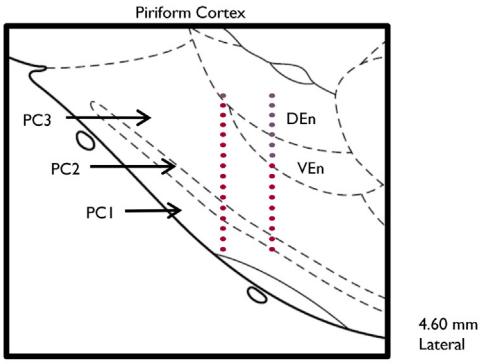

that displays excitatory cortico-thalamocortical connections with the prefrontal cortex, supports it in cognition [25], and may play a potential role in absence epilepsy. The mediodorsal thalamus has demonstrated local pathological changes in the GAERS rat model [26] as well as increase in neuronal firing at the peak of SWDs in the Wistar Albino Glaxo from Rijswijk (WAG/Rij) rat model [27], another well-established animal model of absence epilepsy [28]. Therefore, the piriform cortex to mediodorsal thalamus pathway may contribute to or form part of the absence epilepsy network. In order to investigate whether this pathway is part of the absence epilepsy network, it is necessary to apply a brain connectivity measure.

Brain connectivity measures such as correlation and coherence describe whether two brain regions display similar neuronal firing or oscillatory activity with each other but do not inform whether one brain region is driving activity in the other [29,30]. In this study, we use another form of connectivity named 'effective connectivity'. Effective connectivity is defined as *"…the influence one neural system exerts over another"* [29] and can be applied to EEG and local field potential (LFP) data [31,32]. *Transfer entropy* is a novel measure accounting for 'effective connectivity' and is considered to be equivalent to Granger causality, another effective connectivity measure [33], however, transfer entropy is capable of handling non-Gaussian distributed variables commonly seen in biological data. Transfer entropy has been used to quantify effective connectivity between neurons, and it has also been applied to LFPs to detect changes in connectivity between brain regions in different brain states [34,35]. We used transfer entropy to establish a unidirectional estimate of effective connectivity to evaluate neural oscillatory communication between the piriform cortex to the mediodorsal thalamus. This pathway is a well-defined and validated pathway in the neuroanatomical literature, and we define this pathway as a *strongly direct causal interaction*. We implanted multichannel microelectrode arrays into the piriform cortex and mediodorsal thalamus to record LFPs in GAERS and NEC strains. Our frequency bands of interest were "wide" theta (2–12 Hz), beta (15–35 Hz), and gamma (36–80 Hz) as described in [36] and "narrow" theta (4–8 Hz) because of its reported early changes prior to absence seizure onset [37]. Across frequency bands, we hypothesize that the GAERS strain will exhibit increased effective connectivity, before and during generalized epileptogenic discharges, in the well-characterized neural pathway from piriform cortex to mediodorsal thalamus, compared with the NEC strain.

2. Material and methods

2.1. Experimental setup

Experiments were performed on adult male rats (aged 4–6 months) from the GAERS strain and a NEC strain that were anesthetized using systemic Intraperitoneal (I.P.) injections of urethane (20% vol/vol) until the rats were unconscious. Urethane is considered to be an unbiased anesthetic that affects both excitatory and inhibitory systems [38]. The rats were then placed in a stereotaxic frame with a thermoregulatory head pad to maintain body temperature at 37 °C. Burr holes were drilled over primary motor cortex (left and right) (coordinates: Anterior-Posterior (AP): 10.44 mm, Medial-Lateral (ML): ±3.5 mm, Dorsal-Ventral (DV): 0 mm (dura), angle: 0°) for insertion of stainless steel screw electrodes (Plastics One) for EEG recordings. Imaging demonstrated that screw electrodes were predominantly placed over primary motor cortex with some overlap at the adjacent somatosensory cortex. Screw electrodes have been previously used to verify the cortical manifestation of absence seizure in awake freely moving GAERS [39]. Thirty-two-channel microelectrode arrays (2 shanks with 16 electrodes per shank, distance between electrodes along shank — 100 μm, distance between shank — 500 μm) (Neuronexus) were inserted into the left mediodorsal nucleus of the thalamus (AP: 9.0 mm, ML: −0.6 mm, DV: 6.5 mm, angle: 32.5°) and piriform cortex (AP: 8.2 mm, ML: −4.9 mm, DV: 7.6 mm, angle: 32.5°). Once surgical procedures were completed, rats underwent electrophysiological recordings for approximately 7 h. Following electrophysiological recordings, all animals were put down with an 80 mg/kg dose of sodium pentobarbitone followed by transcardial perfusion with 10% formalin. Rat brains were preserved in 10% formalin. Tissue was sectioned at 10–20 μm and Nissl stained to confirm placement of electrodes (Fig. 1). The placement of microelectrode arrays in the mediodorsal thalamus and piriform cortex was confirmed using landmarks delineated from Paxinos and Watson [40] under a confocal microscope (Nikon, Australia) in 3 subjects while screw electrodes were confirmed via visual inspection. The bottom 16-electrode contacts of both the piriform cortex and mediodorsal thalamus were used for analysis as they were consistently located in the correct position.

A Tucker-Davis Technologies system was utilized in the recording of EEG and LFPs. Recordings were amplified by a PZ2 PreAmp and were preprocessed on a RZ2 BioAmp Processor. Electroencephalography and LFP recordings were sampled at 4069 Hz. All data were stored onto an RS4 Data Streamer for analysis. MATLAB 2017 was used for all postexperimental analysis of EEG and LFP data. All procedures were approved by Animal Ethics Committee at the Florey Institute of Neuroscience and Mental Health (FINMH-17005) in adherence to the Australian Code of Practice for the Care and Use of Animals for Scientific Purposes.

2.2. Detection of generalized epileptiform discharges

We observed high amplitude generalized periodic epileptiform discharges from EEG data recorded from screw electrodes in primary motor cortex. Their spectral content localizes in the 5–9-Hz range. They do not display the typical spike–wave waveform pattern of SWDs observed in conscious GAERS. These epileptiform discharges are not observed in control rats. The left screw electrode in primary motor cortex was used for discharge event detection while the right screw electrode was used to verify that the discharge events were generalized across both hemispheres of the brain. Discharge event detection was conducted using the left screw electrode in primary motor cortex because of the placement of the microelectrode arrays in mediodorsal nucleus of the thalamus and piriform cortex in the left hemisphere of the brain.

The EEG signal recorded from the left primary motor cortex was filtered using a third-order zero-phase Butterworth bandpass filter between frequencies of 5 and 9 Hz, in accordance with their expected spectral localization. The signal was further filtered with a moving average–root mean square filter with a window size of 3 samples. This moving root mean square signal produces distinct peaks where the discharges occur and has been previously applied in the detection of electrophysiological events [41].

Fig. 1. Electrode implantation sites. A) Mediodorsal Thalamus Electrode Placement from Coronal Slices — representations of placements (left, image adapted from Paxinos & Watson [40]) and photomicrograph of placement sites from one subject. B) Piriform Cortex Electrode Placement from Coronal Slice — representations of placements (left, image adapted from Paxinos & Watson [40]) and photomicrograph of placement sites from on subject. C) Electrode Placement from Sagittal View Reconstruction. Legend: red arrow/line — microelectrode array track, blue arrow — landmarks granule dentate gyrus (A) and rhinal fissure (B), red dots — represent electrode track line, MDL — mediodorsal thalamus (lateral), MDC — mediodorsal thalamus (central), mediodorsal thalamus (medial), PC1 — piriform cortex layer I, PC2 — piriform cortex layer II, PC3 — piriform cortex layer III, DEn — dorsal endopiriform cortex, VEn — ventral endopiriform cortex.

The time of onset can be determined by finding the intersection between the moving root mean square signal and a given threshold. The value of this threshold was derived from the empirical cumulative distribution function of 5 s of baseline signal. This baseline period was chosen at the center of an interictal period lasting a minute with no generalized epileptiform discharges present. The 95th percentile of the empirical cumulative distribution function was chosen as the final threshold. The benefit of this method is that it does not assume normality of the energy distribution and has been previously used in high-frequency oscillation detection [42]. For analysis, we used 100 epileptiform discharges from each GAERS and from each NEC rat. We randomly selected 100 recording epochs of one second in duration, which demonstrated no generalized discharge activity.

2.3. Transfer entropy: a measure of effective connectivity

Transfer entropy is a nonparametric statistical measure that quantifies the amount of information that is transferred between two processes (here denoted as X → Y) [43]. It is a measure of effective connectivity or 'causality connectivity' as it predicts the past information of variable, or time-series, X by accounting for the past and future information of variable, or time-series, Y [31].

In accordance with our hypothesis outlined at the end of the Introduction, we calculate transfer entropy between the piriform cortex and the mediodorsal thalamus (see black arrows in Fig. 2). We assume that there is a strong causal interaction between these two brain regions (Piriform Cortex = X and Mediodorsal Thalamus = Y). A single transfer entropy estimate from region X to region Y requires three inputs;: a sample time series (LFPs) from brain region X, a sample time series (LFPs) from region Y, and an estimated time lag from regions X to Y, here using the Darbellay–Vajda adaptive partitioning algorithm [44]. High transfer entropy values indicate strong effective connectivity whereas low transfer entropy values indicate weak effective connectivity.

2.3.1. Global time lag estimation for transfer entropy

A challenging, and important, aspect of transfer entropy is the estimation of a 'time lag'. In other words, how far do we space X and Y from each other (in milliseconds). Transfer entropy with varying time lag estimates may reflect changes in time lag rather than effective connectivity as transfer entropy increases in a logarithmic fashion with an increase in the time lag estimate (see Supplementary material — Fig. 1). It is, therefore, necessary to determine global time lag estimate between X and Y for all connectivity pairs.

A time lag estimate for the pathway from brain regions X to Y can be calculated by performing the cross-correlation of a 1-second sample from brain regions X to Y in a control rat. The number of time lag estimates for each pathway depends on the number of electrode sites in brain regions X and Y. For the pathway of piriform cortex to thalamus, there are a total of 16 electrode sites in each brain regions and, therefore, a total of 256 possible combinations. From 100 sampled seconds from 3 controls, a combined total of 76,800 time lag estimates can be performed for this pathway. The time lag estimates are shown in Fig. 3.

The median value of time lag estimates between 5 and 50 ms was selected as the global time lag estimate between brain regions (red arrow in Fig. 3). Previously estimated time lags between brain sites applying a cross-correlation to LFPs have shown to be below 50 ms [45,46] whereas short lag estimates of less than 5 ms are considered to represent synchronous, and not effective, connectivity and produces a transfer entropy estimate close to 0. The global time lag estimate computed with these assumptions was 20.9 ms for piriform cortex to mediodorsal thalamus.

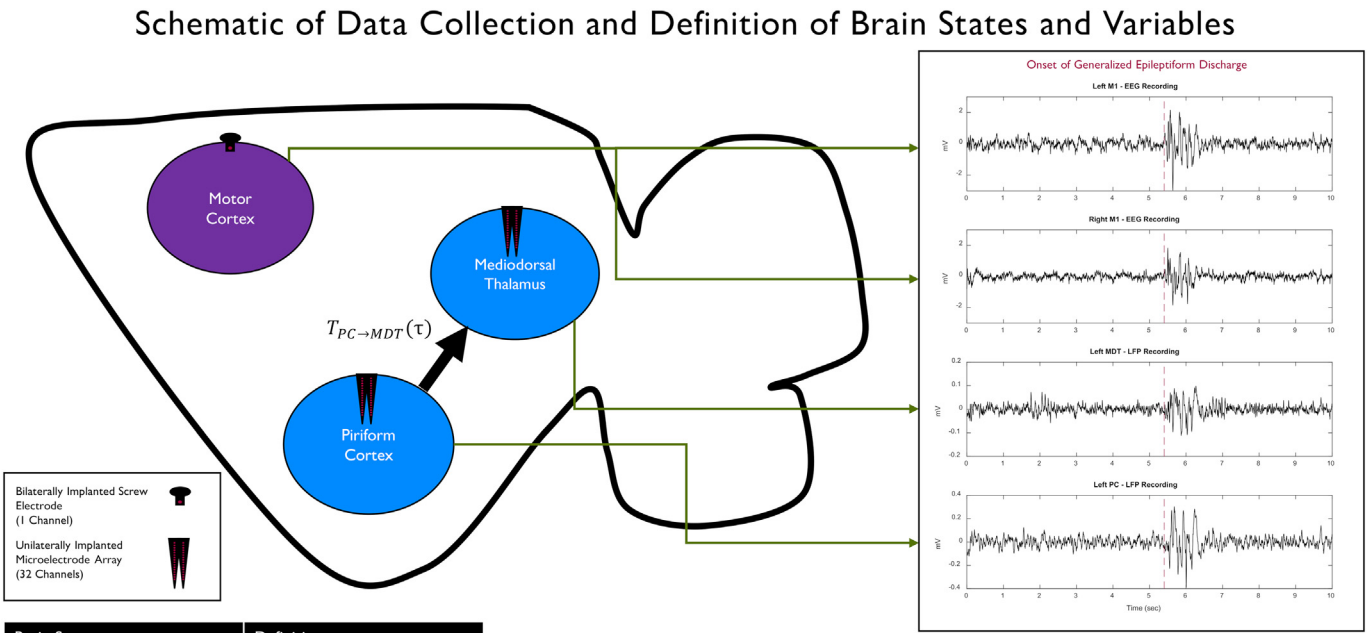

Brain State	Definition
Pre-Onset	1 second prior to onset of SWD from GAERS
Onset	First second of SWD onset from GAERS
Control	1 second randomly sampled from NEC

Fig. 2. Schematic of data collection and definitions of brain states and variables. M1 — primary motor cortex, MDT — mediodorsal thalamus, PC — piriform cortex. $T_{PC\rightarrow MDT}(\tau)$ — transfer entropy from piriform cortex to mediodorsal thalamus for a time lag τ. Bilaterally implanted screw electrodes in motor cortex were used to reliably delineate epileptogenic discharges.

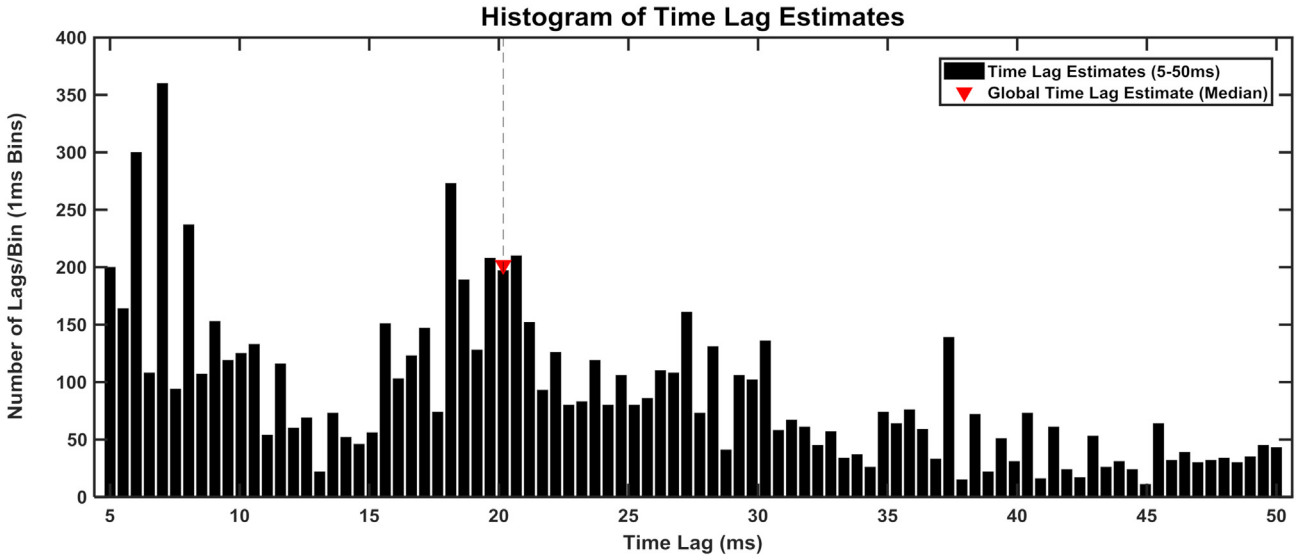

Fig. 3. Histogram of estimated time lags for piriform cortex to mediodorsal thalamus pathway with global time lag estimate (red arrow). Time lag estimates produces by cross-correlograms of piriform cortex and mediodorsal thalamus LFP signals for the control rats (76,800 estimates in total).

2.3.2. Transfer entropy construction

For each global time lag estimate, transfer entropy can be calculated as follows. From two evenly sized sampled time series, $X = \{x_1, x_2, \ldots, x_N\}$ and $Y = \{y_1, y_2, \ldots, y_N\}$, the transfer entropy from X to Y ($T_{X\to Y}$) can be derived from conditional entropies as shown below in Eqs. (1) and (2) [44].

$$T_{X\to Y} = H\left(y_i|y_{i-t}^{(n)}\right) - H\left(y_i|y_{i-t}^{(n)}, x_{i-\tau}^{(m)}\right) \tag{1}$$

$$T_{X\to Y} = \sum_{y_i, y_{i-t}^{(n)}, x_{i-\tau}^{(k)}} p\left(y_i, y_{i-t}^{(n)}, x_{i-t}^{(m)}\right) \log \frac{p\left(y_i|y_{i-t}^{(n)}, x_{i-\tau}^{(m)}\right)}{p\left(y_i|y_{i-t}^{(n)}\right)} \tag{2}$$

where τ and t are the time lags in X and Y, respectively, and m and n are the block lengths of previous values in X and Y, respectively. i indicates a given point in time. $x_{i-t}^{(m)}$ and $y_{i-t}^{(n)}$ are the past values in the conditional probabilities are defined as follows in Eqs. (3) and (4) [44].

$$x_{i-\tau}^{(m)} = \{x_{i-\tau-l+1}, x_{i-\tau-l+2}, \ldots, x_{i-\tau}\} \tag{3}$$

$$y_{i-t}^{(n)} = \{y_{i-t-l+1}, y_{i-t-l+2}, \ldots, y_{i-t}\} \tag{4}$$

Eqs. (1) and (2) infer that transfer entropy measures the decrease in uncertainty in y_i given $x_{i-t}^{(m)}$ and $y_{i-t}^{(n)}$ in comparison with given only $y_{i-t}^{(n)}$ and is the most commonly applied definition of transfer entropy. Transfer entropy cannot be less than zero as $H(y_i|y_{i-t}^{(n)}) \geq H(y_i|y_{i-t}^{(n)}, x_{i-\tau}^{(m)})$.

To simplify Eq. (2), the values of m and n are set to 1 to account for computing short time series lengths, and t can also be set to 1 assuming that the maximum auto-transfer of information occurs from the time point preceding the target value in Y. These assumptions allow for transfer entropy to be simplified as a function of time delay τ as shown Eq. (5).

$$T_{X\to Y}(\tau) = \sum_{y_i, y_{i-1}, x_{i-\tau}} p(y_i, y_{i-1}, x_{i-\tau}) \log \frac{p(y_i, y_{i-1}, x_{i-\tau}) p(y_{i-1})}{p(y_{i-1}, x_{i-\tau}) p(y_i, y_{i-1})} \tag{5}$$

The joint probabilities of the transfer entropy can be calculated using different methods of probability density function estimation. The Darbellay–Vajda adaptive partitioning algorithm extended to three dimensions has shown to be sensitive to fixed-binning with ranking and has a fast computational time. The main strength of the Darbellay–Vajda adaptive partitioning algorithm is that it needs fewer parameters compared with other methods such as kernel density estimation [44] — it only requires two signals (X and Y) and a time lag estimate (τ).

Darbellay–Vajda algorithm utilizes a three-dimensional space for transfer entropy estimation through recursive partitioning [44]. This three-dimensional space can be defined by v_i, v_{i-1} and $u_{i-\tau}$ into cubes of differing sizes. The initial space is segmented into 8 cubes with the boundaries being the mid-points in the three dimensions. The chi-square statistic is calculated to test the null hypothesis that the data points are evenly distributed across the 8 cubes.

$$s_{X^2} = \sum_{i=1}^{8} (M_i - \mu_M)^2 \tag{6}$$

M_1, M_2 … M_8 are the numbers of data points contained in the 8 cubes, and μ_M is the average of the data points over the 8 cubes. If $s_{X^2} > X^2_{95\%}$ (greater than 95% confidence), then the null hypothesis is rejected, and each of the 8 cubes is further partitioned into 8 smaller cubes. This recursive process will continue as such until the null hypothesis is not rejected. When the null hypothesis is not rejected, the partitions in the present iteration are disregarded, and the current 8 cubes being analyzed are taken as a single partition. If cubes contain no data points, they have no influence on the transfer entropy.

Partitioning results in a fixed number of cubes, L, containing data points not equal to 0. $T_{X\to Y}$ can now be estimated using L partitions as follows:

$$T_{X\to Y}(\tau) \approx \sum_{k=1}^{L} \frac{nk}{P} \log \frac{\left(n_k n_k^{y_i - 1}\right)}{\left(n_k^{y_i - 1, x_i - \tau} n_k^{y_i, y_i - 1}\right)} \tag{7}$$

P is the total number of data triplets (y_i, y_{i-1}, $x_{i-\tau}$), and n_k is the number of data points in the kth partition. $n_k^{y_{i-1}}$, $n_k^{y_i-1, x_i-\tau}$, $n_k^{y_i, y_i-1}$ are the number of data points that lie between the lower and upper bounds of the kth partition in the total data set.

Table 1
Summary of parameters and variables for transfer entropy application.

Parameters	Definition	Abbreviations
Pathway	Pathway of effective information. PC to MDT	X → Y where X = PC and Y = MDT PC → MDT
Range	Spectral range for third order Butterworth bandpass filtering of signals from X and Y.	"Wide" theta (2–12 Hz) "Narrow" theta (4–8 Hz) Beta (15–35 Hz) Gamma (36–80 Hz)
State	1 s prior to the onset of a discharge First second of discharge onset 1 random second sample from control	Pre-onset Onset Control
Strain	Animal strain	GAERS NEC

Variables		Values
τ	Global time lag estimate for a given pathway	20.9 ms for PC → MDT
k	**Combination** number of signals X^a and Y^b as defined in Global Time Lag Estimation Section	k = 1, 2, 3 … 256 for PC → MDT
s	**Sample** number of either discharges or randomly second samples from control	s = 1, 2, 3 … 100
r	**Subject** number of either GAERS or NEC	r = 1, 2, 3

PC — piriform cortex, MDT — mediodorsal thalamus.

2.3.3. Transfer entropy application

The application of transfer entropy estimations is conducted in a similar fashion to the estimation of time lags. Transfer entropy can be estimated for each combination of electrodes *k* over 100 brain state samples *s* for 3 rats of each strain *r*. These variables along with a time lag estimate τ along with input signal type parameters can be written as shown in Eq. (8) below and is summarized in Table 1.

$$T_{X\to Y}(\tau) = T_{Pathway,Range,State,Strain}(\tau, k, s, r) \tag{8}$$

2.4. Statistical analysis

For each frequency, the median transfer entropy score for each subject and brain state was used for group level analysis. We perform two unpaired t-tests: i) between pre-onset (GAERS) and control states (NEC) and ii) between onset (GAERS) and control states (NEC). Because of the small sample size, we reported t-values and uncorrected probability values at $p < 0.05$. Bonferroni-corrected threshold for three multiple comparisons in each frequency band is $p < 0.0167$.

3. Results

3.1. Transfer entropy — theta effective connectivity

There was greater effective connectivity of pre-onset states versus the control states for "wide" theta band transfer entropy ($t(4) = 2.4604$, $p < 0.05$). There were no changes between pre-onset and control ($t(2) = 1.921$, $p = 0.097$) or onset and control ($t(2) = 2.729$, $p = 0.056$) for the piriform cortex and mediodorsal thalamus pathway. In the "narrow" theta band, there was greater effective connectivity in the pre-onset versus control states ($t(2) = 3.313$, $p < 0.05$) while there were trending changes between onset and control states ($t(2) = 2.920$, $p = 0.050$) and no changes between pre-onset and onset states ($t(4) = 0.582$, $p = 0.296$). These results are displayed in Fig. 4.

3.2. Transfer entropy — beta and gamma effective connectivity

In the beta band, there was greater effective connectivity in onset versus pre-onset states ($t(4) = 11.018$, $p < 0.0167$) and also a trend increase in effective connectivity in the onset versus control states ($t(2) = 2.684$, $p = 0.058$), between the piriform cortex and mediodorsal thalamus. However, there was no difference between pre-onset and control states ($t(2) = 0.609$, $p = 0.302$). Similarly, the gamma band demonstrated increased effective connectivity in onset states compared with the pre-onset states ($t(4) = 9.216$, $p < 0.0167$) and also greater effective connectivity in onset states versus the control states ($t(2) = 3.927$, $p < 0.05$). There was no difference between pre-onset and control states ($t(2) = 1.812$, $p = 0.106$) (Fig. 5).

4. Discussion

In line with our hypothesis, we observed increased theta, beta, and gamma effective connectivity from the piriform cortex to the mediodorsal thalamus, during the onset of epileptic brain states. We also observed trending increase in theta effective connectivity during pre-onset brain states in this pathway. These findings suggest that this well-characterized neural pathway between piriform cortex and mediodorsal thalamus may be recruited as part of the 'absence epilepsy network'.

4.1. Theta effective connectivity

Increased "narrow" theta effective connectivity from piriform cortex to mediodorsal thalamus may suggest that olfactory networks are also a part of the wider 'epileptic network' in genetic absence epilepsy. This may be due to the localization of generalized epileptiform discharges within this low frequency spectral band, suggesting that this pathway may be predisposed to propagate this epileptogenic activity in GAERS. Piriform cortex is the critical node of the olfactory network. This network is thought to be mediated by glomerular layer interneurons in the olfactory bulb [47]. Periglomerular cells have shown to be coupled with respiration rhythm, and their feedforward inhibition is considered to be an underlying mechanism of the phase delay of mitral cells that may be used to project olfactory bulb activity to the piriform cortex. This may be due to changes in respiration prior to and during the onset of absence seizures as has been previously reported in animal and human studies [48,49]. Recordings of cardiac and respiratory rate are needed to verify whether theta effective connectivity is correlated with changes in the autonomic system. Furthermore, theta oscillations have also shown to convey odor-specific content in the piriform cortex [50]. Increases in theta band power have been observed in the thalamus in response to an odor [36]. While discharges localize in a narrow band of these "wide" theta oscillations, there are no reported cases of olfactory dysfunction or auras in absence epilepsy. This may explain why there is a minimal impact on the olfactory function of patients with absence epilepsy, in contrast to the findings in focal epilepsy cases. Impaired consciousness during absence seizures may result in patients not remembering olfactory

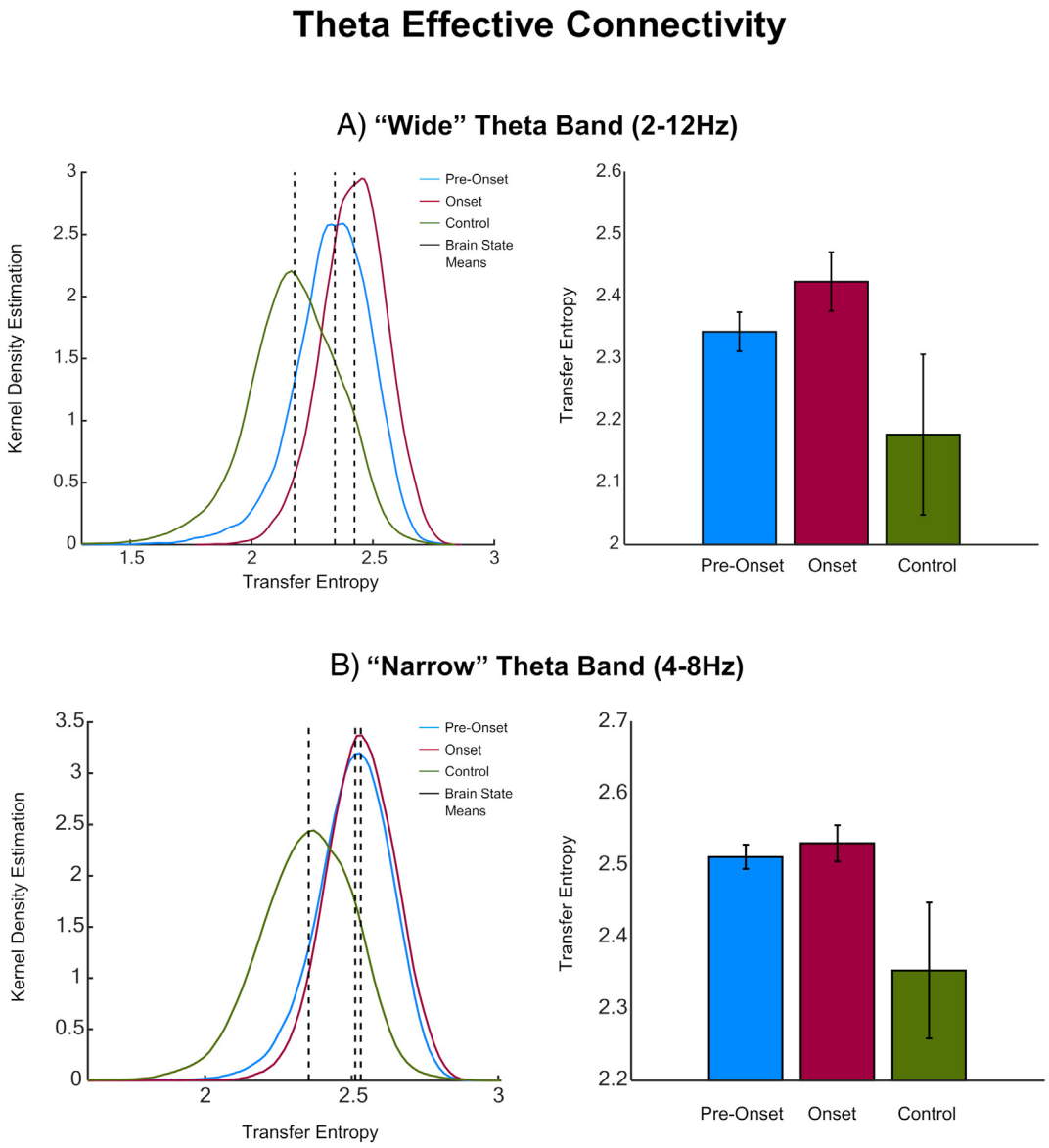

Fig. 4. Results for Theta effective connectivity of the piriform cortex to mediodorsal thalamus pathway. A) Results for "wide" theta band. B) Results for "narrow" theta band. The left column displays the kernel density estimate of the raw transfer entropy estimates with mean values;. The right column displays the bar plots of the brain states with error bars (standard deviation).

hallucinations prior to seizure onset. Furthermore, seizures have shown to involve the piriform cortex without the presence of olfactory hallucination [51]. Therefore, this pathway may be recruited without having a significant impact on olfactory function, or olfactory hallucinations may not be recalled.

4.2. Beta and gamma effective connectivity

The increase in effective connectivity during discharge onset for the beta band indicates hyperexcitability within the piriform–thalamic pathway. Piriform cortex projections to the mediodorsal thalamus are predominantly glutamatergic and excitatory [52]. Given that there is no observable change between pre-onset and control brain states, we postulate that beta-mediated communication between piriform cortex and mediodorsal thalamus is unchanged. Beta oscillations are known to be generated in both piriform cortex and mediodorsal thalamus after application of an odor stimulus, with 67% of mediodorsal thalamus single units phase-locked to piriform cortex beta oscillations [36]. The information transfer of beta oscillations is also thought to extend to the orbitofrontal cortex's connections to both piriform cortex and mediodorsal thalamus [53]. The orbitofrontal cortex receives direct sensory inputs from the somatosensory cortex [54], which may result in remote modulation of beta oscillatory communication between the piriform cortex and mediodorsal thalamus during epileptiform discharges.

The increase in gamma band effective connectivity was shown to be trending from pre-onset to onset similar to the trending increase in beta band effective connectivity. The olfactory bulb has shown to display gamma oscillations that are either elicited by olfactory stimuli or are spontaneously evoked [55]. Olfactory receptor neurons in the olfactory bulb are glutamatergic and generate action potentials that travel along the olfactory nerve fiber onto mitral and tuft cells. Inhibition of gamma activity is caused by granule cells that cause gamma oscillations to occur [47]. The piriform cortex is known to receive very dense inputs from olfactory bulb mitral and tuft cells in its anterior section, which in turn projects strongly to the mediodorsal thalamus resulting in the observation of gamma oscillations in these regions [36,56]. Discharge propagation via excitatory pyramidal neurons in cortical regions such as the orbitofrontal cortex may, in turn, excite the highly interconnected pyramidal neurons in the piriform cortex.

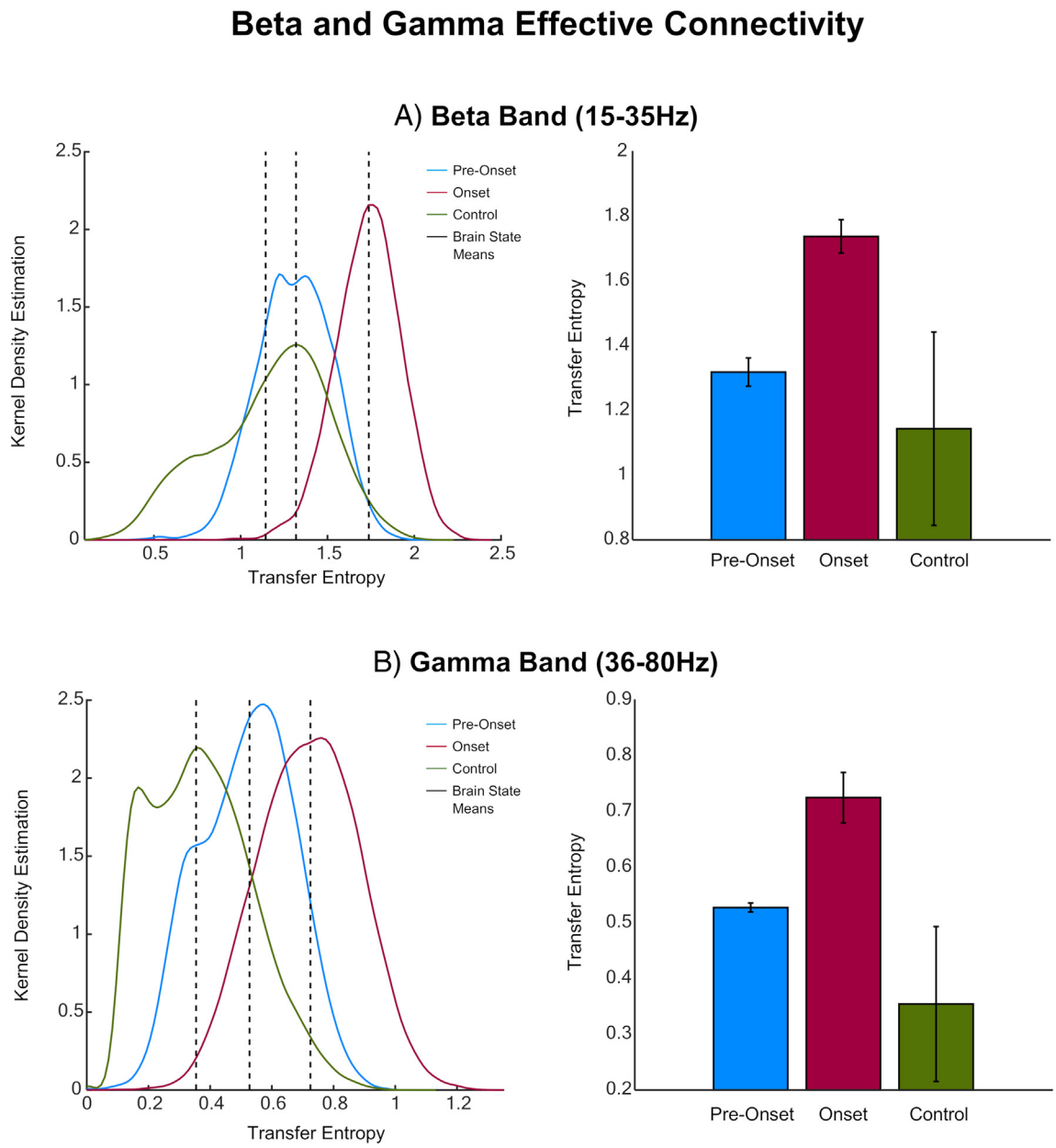

Fig. 5. Results for beta and gamma effective connectivity for piriform cortex to mediodorsal thalamus pathway. A) Results for "wide" theta band. B) Results for "narrow" theta band. The left column displays the kernel density estimate of the raw transfer entropy estimates with mean values;. The right column displays the bar plots of the brain states with error bars (standard deviation).

4.3. Clinical implications

The piriform cortex and mediodorsal thalamus are more commonly associated with temporal lobe epilepsies compared with absence epilepsy [57,58]. A recent paper by Galovic et al. demonstrated resection of at least half the piriform cortex increased the odds of seizure freedom compared with other limbic structures resected [59]. This highlights the involvement of the piriform cortex in temporal lobe epilepsy, and there is also preliminary evidence to suggest that it may be a desirable target for deep brain stimulation (DBS) for treatment of epilepsy [60,61]. We previously discussed how the piriform cortex may be connected with the absence epilepsy network and how it may serve as a DBS target for absence epilepsy [19]. Preliminary evidence suggests that mediodorsal thalamus may be a suboptimal DBS target for the treatment of mesial temporal lobe seizures [62], but it has been proposed as the optimal target for DBS in patients with Lennox–Gastaut syndrome who often display EEG spike and slow wave discharges [63]. Future studies should investigate the local changes within the piriform cortex and mediodorsal thalamus in absence epilepsy as well as their relationship with other regions involved in the absence epilepsy network prior to testing intervention strategies such as DBS.

4.4. Limitations

The main challenge for transfer entropy estimation is its global time lag estimate — i.e., *how far apart we space signals from brain regions X and Y (in time) to estimate their transfer of information*. One of our key observations in determining the global time lag estimate was the distribution of time lag estimations for each of the pathways under investigation. We observed sporadic estimations of time lag for the primary motor to piriform cortex pathway in comparison with the clustering around the median estimates for the other pathways. This indicates that transfer entropy is best suited to directly connected pathways with reliable time lag estimations. Alternative methods of time lag estimation

compared with cross correlation could be applied, however, large variations in time lag estimation will still strongly influence transfer entropy estimations.

The generalized epileptiform discharges we detected were shorter in duration and did not display the typical spike and wave characteristics as commonly observed in awake freely moving GAERS [39]. This is likely the result of urethane's suppressive effect on thalamic relay neurons [64]. Future studies should endeavor to conduct chronic recordings to observe these effective connectivity changes in conscious GAERS.

In this study, we tested exploratory hypotheses regarding the role of the piriform cortex and mediodorsal thalamus in generalized epileptic discharges, and we, therefore, decided to only use three GAERS and control rats to avoid needless waste of animals and resources. Although similar animal numbers are found in multielectrode studies [65,66], our results should be treated as preliminary, and further research is needed to validate the generalizability and reproducibility of these findings. Finally, it would be of interest to study whether there are pathological network differences between GAERS or NECs by comparing interictal brain states with control brain states in future studies.

5. Conclusions

The application of transfer entropy to determine the effective connectivity between subcortical structures that are directly connected in an epileptic animal model is a novel endeavor. With a global time lag estimate, it is simple to implement and can provide insight into how communication from one brain region to another occurs via functional spectral bands. From our preliminary findings, this method of investigating effective connectivity could be applied to the study of other epileptic networks and neurological disorders.

Author contributions

Authors had full access to all data and take responsibility of the presented data. Prof. Antonio G. Paolini and James C. Young designed and performed the experiments together. James Young analyzed all of the data acquired. All authors interpreted the data and were involved in drafting and revising of the article with respect to intellectual content. The study was supervised by Prof. Antonio Paolini and Prof. Graeme D Jackson.

Declaration of Competing Interest

The authors declare that the research was conducted in the absence of any commercial or financial relationship that could be construed as a potential conflict of interest.

Acknowledgments

We thank Angela Lim for assistance in electrophysiology recording monitoring and aiding in transcardial perfusion and Dr. Helen Nasser for her assistance with performing histology. We also acknowledge Prof. Terence O'Brien and Dr. Pablo Casilla-Espinosa for providing GAERS and NEC rats for this study. The Florey Institute of Neuroscience and Mental Health acknowledges the strong support from the Victorian Government in particular the funding from the Operational Infrastructure Support Grant. This study was supported by the National Health and Medical Research Council of Australia (NHMRC Project Grant 1091593). James C Young acknowledges that they have been supported through an Australian Government Research Training Program Scholarship.

Appendix A. Supplementary data

Supplementary data to this article can be found online at https://doi.org/10.1016/j.yebeh.2019.05.042.

References

[1] Crunelli V, Leresche N. Childhood absence epilepsy: genes, channels, neurons and networks. Nat Rev Neurosci 2002;3:371–82.
[2] Blumenfeld H. Consciousness and epilepsy: why are patients with absence seizures absent? Prog Brain Res 2005;150:271–86.
[3] Pinault D, Slézia A, Acsády L. Corticothalamic 5–9 Hz oscillations are more pro-epileptogenic than sleep spindles in rats. J Physiol 2006;574:209–27.
[4] Westmijse I, Ossenblok P, Gunning B, Luijtelaar GV. Onset and propagation of spike and slow wave discharges in human absence epilepsy: a MEG study. Epilepsia 2009; 50:2538–48.
[5] Meeren HKM, Pijn JPM, Van Luijtelaar ELJM, Coenen AML, Lopes da Silva FH. Cortical focus drives widespread corticothalamic networks during spontaneous absence seizures in rats. J Neurosci Off J Soc Neurosci 2002;22:1480–95.
[6] Blumenfeld H. Cellular and network mechanisms of spike–wave seizures. Epilepsia 2005;46(Suppl. 9):21–33.
[7] Carney PW, Masterton RA, Harvey AS, Scheffer IE, Berkovic SF, Jackson GD. The core network in absence epilepsy: differences in cortical and thalamic BOLD response. Neurology 2010;75:904–11.
[8] Carçak N, Ferrandon A, Koning E, Aker RG, Ozdemir O, Onat FY, et al. Effect of stage 2 kindling on local cerebral blood flow rates in rats with genetic absence epilepsy. Epilepsia 2009;50:33–43.
[9] Akhmadeev AV, Nagaeva DV, Kalimullina LB. The paleoamygdala: comparative analysis of its structural-functional organization in WAG/Rij and Wistar rats. Neurosci Behav Physiol 2013:682.
[10] Jafarian M, Karimzadeh F, Alipour F, Attari F, Lotfinia AA, Speckmann EJ, et al. Cognitive impairments and neuronal injury in different brain regions of a genetic rat model of absence epilepsy. Neuroscience 2015;298:161–70.
[11] Arcaro J, Ma J, Chu L, Kuo M, Mirsattari SM, Stan Leung L. The hippocampus participates in a pharmacological rat model of absence seizures. Epilepsy Res 2016;120: 79–90.
[12] Onat FY, van Luijtelaar G, Nehlig A, Snead III OC. The involvement of limbic structures in typical and atypical absence epilepsy; 2013; 111–23.
[13] Vaughan D, Warren A, Carney P, Abbott D, Archer J, Jackson G. Timing and laterality of piriform cortex activation in focal and generalized epilepsies. 21st Organization for Human Brain Mapping Conference. Honolulu, Hawaii; 2015.
[14] Tondelli M, Vaudano AE, Ruggieri A, Meletti S. Cortical and subcortical brain alterations in juvenile absence epilepsy. Neuroimage Clin 2016;12:306–11.
[15] Löscher W, Ebert U. The role of the piriform cortex in kindling. Prog Neurobiol 1996; 50:427–81.
[16] Depaulis A, David O, Charpier S. The genetic absence epilepsy rat from Strasbourg as a model to decipher the neuronal and network mechanisms of generalized idiopathic epilepsies. J Neurosci Methods 2016:159.
[17] Marescaux C, Vergnes M, Depaulis A. Genetic absence epilepsy in rats from Strasbourg—a review. J Neural Transm Suppl 1992;35:37–69.
[18] Marks WN, Cavanagh ME, Greba Q, Cain SM, Snutch TP, Howland JG. The Genetic Absence Epilepsy Rats from Strasbourg model of absence epilepsy exhibits alterations in fear conditioning and latent inhibition consistent with psychiatric comorbidities in humans; 2016; 25–40.
[19] Young JC, Vaughan DN, Paolini AG, Jackson GD. Electrical stimulation of the piriform cortex for the treatment of epilepsy: a review of the supporting evidence. Behavior; Epilepsy Behav 2018;88:152–61.
[20] Cornwall J, Phillipson OT. Afferent projections to the dorsal thalamus of the rat as shown by retrograde lectin transport—I. The mediodorsal nucleus. Neuroscience 1988;24:1035–49.
[21] Powell TPS, Cowan WM, Raisman G. Olfactory relationships of the diencephalon. Nature 1963;199:710.
[22] Price JL. Beyond the primary olfactory cortex: olfactory-related areas in the neocortex, thalamus and hypothalamus. Chem Senses 1985;10:239.
[23] Bay HH, Cavdar S. Regional connections of the mediodorsal thalamic nucleus in the rat. Imperial College Press2013 201.
[24] Kuroda M, López-Mascaraque L, Price JL. Neuronal and synaptic composition of the mediodorsal thalamic nucleus in the rat: a light and electron microscopic Golgi study. J Comp Neurol 1992;326:61–81.
[25] Mitchell AS. The mediodorsal thalamus as a higher order thalamic relay nucleus important for learning and decision-making. Neurosci Biobehav Rev 2015;54:76–88.
[26] Çavdar S, Özgür M, Kirazlı Ö, Karahüseyinoğlu S, Onat F. Comparing glutamatergic neuron population in the mediodorsal thalamic nucleus of genetic absence epilepsy rats from Strasbourg (GAERS) and normal control Wistar rats. J Chem Neuroanat 2016;77:93–9.
[27] Inoue M, Duysens J, Vossen JM, Coenen AM. Thalamic multiple-unit activity underlying spike–wave discharges in anesthetized rats. Brain Res 1993;612:35–40.
[28] Russo E, Citraro R, Constanti A, Leo A, Lüttjohann A, van Luijtelaar G, et al. Review article: upholding WAG/Rij rats as a model of absence epileptogenesis: hidden mechanisms and a new theory on seizure development. Neurosci Biobehav Rev 2016;71:388–408.
[29] Friston KJ. Functional and effective connectivity: a review. Brain Connect 2011;1: 13–36.
[30] Bowyer SM. Coherence a measure of the brain networks: past and present. Neuropsychiatric Electrophysiology 2016;2(1).
[31] Timme NM, Lapish C. A tutorial for information theory in neuroscience. eNeuro 2018;5:ENEURO.0052-18.2018.
[32] Vicente R, Wibral M, Lindner M, Pipa G. Transfer entropy—a model-free measure of effective connectivity for the neurosciences. J Comput Neurosci 2011;30:45–67.
[33] Barnett L, Barrett AB, Seth AK. Granger causality and transfer entropy are equivalent for Gaussian variables; 2009.

[34] Li Z, Li X. Estimating temporal causal interaction between spike trains with permutation and transfer entropy. Plos One 2013;8:e70894.
[35] Ma C, Pan X, Wang R, Sakagami M. Estimating causal interaction between prefrontal cortex and striatum by transfer entropy. Cogn Neurodyn 2013;7:253–61.
[36] Courtiol E, Wilson DA. Thalamic olfaction: characterizing odor processing in the mediodorsal thalamus of the rat. J Neurophysiol 2014;111:1274–85.
[37] Sitnikova E, van Luijtelaar G. Electroencephalographic precursors of spike-wave discharges in a genetic rat model of absence epilepsy: power spectrum and coherence EEG analyses. Epilepsy Res 2009;84:159–71.
[38] Hara K, Harris RA. The anesthetic mechanism of urethane: the effects on neurotransmitter-gated ion channels. United States: WILLIAMS AND WILKINS; 2002; 313.
[39] Kadam SD, D'Ambrosio R, Duveau V, Roucard C, Garcia-Cairasco N, Ikeda A, et al. Methodological standards and interpretation of video-electroencephalography in adult control rodents. A TASK1-WG1 report of the AES/ILAE Translational Task Force of the ILAE. Epilepsia 2017;58(Suppl. 4):10–27.
[40] Paxinos G, Watson C. The rat brain in stereotaxic coordinates/George Paxinos, Charles Watson. San Diego: Academic Press; 1998 c1998.
[41] Staba RJ, Wilson CL, Bragin A, Fried I, Engel Jr J. Quantitative analysis of high-frequency oscillations (80–500 Hz) recorded in human epileptic hippocampus and entorhinal cortex. J Neurophysiol 2002;88:1743–52.
[42] Gardner AB, Worrell GA, Marsh E, Dlugos D, Litt B. Human and automated detection of high-frequency oscillations in clinical intracranial EEG recordings. Clin Neurophysiol 2007;118:1134–43.
[43] Schreiber T. Measuring information transfer. Phys Rev Lett 2000;85:461–4.
[44] Lee J, Nemati S, Silva I, Edwards BA, Butler JP, Malhotra A. Transfer entropy estimation and directional coupling change detection in biomedical time series. Biomed Eng Online 2012;11:19.
[45] Adhikari A, Sigurdsson T, Topiwala MA, Gordon JA. Cross-correlation of instantaneous amplitudes of field potential oscillations: a straightforward method to estimate the directionality and lag between brain areas. J Neurosci Methods 2010;191:191–200.
[46] Soltanzadeh MJ, Daliri MR. Evaluation of phase locking and cross correlation methods for estimating the time lag between brain sites: a simulation approach. Basic Clin Neurosci 2014;5:205–11.
[47] Fukunaga I, Herb JT, Kollo M, Boyden ES, Schaefer AT. Independent control of gamma and theta activity by distinct interneuron networks in the olfactory bulb. Nat Neurosci 2014;17:1208–16.
[48] Jansen K, Varon C, Van Huffel S, Lagae L. Ictal and interictal respiratory changes in temporal lobe and absence epilepsy in childhood. Epilepsy Res 2013;106:410–6.
[49] Roche-Labarbe N, Zaaimi B, Mahmoudzadeh M, Osharina V, Wallois A, Nehlig A, et al. NIRS-measured oxy- and deoxyhemoglobin changes associated with EEG spike-and-wave discharges in a genetic model of absence epilepsy: the GAERS. Epilepsia 2010;51:1374–84.
[50] Jiang H, Schuele S, Rosenow J, Zelano C, Parvizi J, Tao JX, et al. Theta oscillations rapidly convey odor-specific content in human piriform cortex. Neuron 2017;94:207–219.e4.
[51] Vaudano AE, Carmichael DW, Salek-Haddadi A, Rampp S, Stefan H, Lemieux L, et al. Networks involved in seizure initiation. A reading epilepsy case studied with EEG-fMRI and MEG. Neurology 2012;79:249–53.
[52] Ray JP, Russchen FT, Fuller TA, Price JL. "Transmitter specific" inputs to the mediodorsal thalamic nucleus in the rat. In: Ferrendelli JA, Collins RC, Johnson EM, editors. Neurobiology of amino acids, peptides and trophic factors. Boston, MA: Springer US; 1988. p. 243–4.
[53] Plailly J, Howard JD, Gitelman DR, Gottfried JA. Attention to odor modulates thalamocortical connectivity in the human brain. J Neurosci Off J Soc Neurosci 2008;28:5257–67.
[54] Rolls ET. Convergence of sensory systems in the orbitofrontal cortex in primates and brain design for emotion. Anat Rec A Discov Mol Cell Evol Biol 2004;281:1212–25.
[55] Rojas-Líbano D, Kay LM. Olfactory system gamma oscillations: the physiological dissection of a cognitive neural system. Cogn Neurodyn 2008;2:179–94.
[56] Carmichael JE, Gmaz JM, van der Meer MAA. Gamma oscillations in the rat ventral striatum originate in the piriform cortex. J Neurosci 2017;37:7962.
[57] Vaughan DN, Jackson GD. The piriform cortex and human focal epilepsy. Front Neurol 2014;5:1–18.
[58] Patel S, Millan MH, Meldrum BS. Decrease in excitatory transmission within the lateral habenula and the mediodorsal thalamus protects against limbic seizures in rats. Exp Neurol 1988;101:63–74.
[59] Galovic M, Baudracco I, Wright-Goff E, Pillajo G, Nachev P, Wandschneider B, et al. Association of piriform cortex resection with surgical outcomes in patients with temporal lobe epilepsy; 2019.
[60] Bayat A, Skopin MD, Joshi S, Siddu M, Mukharesh L, Jahan S, et al. Effects of low-frequency electrical stimulation of the anterior piriform cortex on kainate-induced seizures in rats. Behavior;Epilepsy Behav 2017;72:1–7.
[61] Zhu-Ge ZB, Zhu YY, Wu DC, Wang S, Liu LY, Hu WW, et al. Unilateral low-frequency stimulation of central piriform cortex inhibits amygdaloid-kindled seizures in Sprague–Dawley rats. Neuroscience 2007;146:901–6.
[62] Wang S, Wu D-C, Fan X-N, Zhu M-Z, Hu Q-Y, Zhou D, et al. Mediodorsal thalamic stimulation is not protective against seizures induced by amygdaloid kindling in rats. Neurosci Lett 2010;481:97–101.
[63] Warren AEL, Abbott DF, Jackson GD, Archer JS. Thalamocortical functional connectivity in Lennox–Gastaut syndrome is abnormally enhanced in executive-control and default-mode networks. Epilepsia 2017;58:2085–97.
[64] Huh Y, Cho J. Urethane anesthesia depresses activities of thalamocortical neurons and alters its response to nociception in terms of dual firing modes. Front Behav Neurosci 2013;7.
[65] Shivdasani MN, Mauger SJ, Rathbone GD, Paolini AG. Neural synchrony in ventral cochlear nucleus neuron populations is not mediated by intrinsic processes but is stimulus induced: implications for auditory brainstem implants. J Neural Eng 2009;6:065003.
[66] Allitt BJ, Harris AR, Morgan SJ, Clark GM, Paolini AG. Research paper: thin-film micro-electrode stimulation of the cochlea in rats exposed to aminoglycoside induced hearing loss. Hear Res 2016;331:13–26.